Biophysical Journal
Article

Biophysical Society

The Dynamic Behavior of the $P2X_4$ Ion Channel in the Closed Conformation

Gustavo Pierdominici-Sottile,[1,*] Luciano Moffatt,[2] and Juliana Palma[1]
[1]Departamento de Ciencia y Tecnología, Universidad Nacional de Quilmes, CONICET, Buenos Aires, Argentina; and [2]Instituto de Química Física de los Materiales, Medio Ambiente y Energía, Facultad de Ciencias Exactas y Naturales, Universidad de Buenos Aires, Buenos Aires, Argentina

ABSTRACT We present the results of a detailed molecular dynamics study of the closed form of the $P2X_4$ receptor. The fluctuations observed in the simulations were compared with the changes that occur in the transition from the closed to the open structure. To get further insight on the opening mechanism, the actual displacements were decomposed into interchain motions and intrachain deformations. This analysis revealed that the iris-like expansion of the transmembrane helices mainly results from interchain motions that already take place in the closed conformation. However, these movements cannot reach the amplitude required for the opening of the channel because they are impeded by interactions occurring around the ATP binding pocket. This suggests that the union of ATP produces distortions in the chains that eliminate the restrictions on the interchain displacements, leading to the opening of the pore.

INTRODUCTION

P2X receptors are a family of nonselective cationic channels whose opening is triggered by the binding of ATP to the extracellular domain (1). They are widespread in the tissues of mammals and have an extensive range of functions (2). These receptors are involved in synaptic transmission (3), presynaptic modulation (4), pain signaling (5), taste sensing (6), smooth muscle contraction (7), gastrointestinal motility (8), immune system regulation (9), inflammatory processes (10), cardiovascular responses (11), and tumor development (12,13), among others. For this reason they are regarded as suitable potential targets for development of drugs against pathologies such as chronic neuropathies, inflammatory pain, depression, cystic fibrosis, irritable bowel syndrome, urinary disorders, and cancer (8,14–16). Understanding how these receptors work, at the molecular level, would help to design therapeutic agents to relieve or even cure diseases in which they are involved.

P2X receptors are either homo or heterotrimeric structures (17,18). Human genome codes for seven alternative subunits of these receptors (19) which are labeled with numbers from 1 to 7 ($P2X_1$, $P2X_2$, …, $P2X_7$). So far only the crystal structure of $P2X_4$ has been reported, and both the closed (20) and open conformations (21) have been disclosed. The analysis of these structures has confirmed previous findings about the residues involved in ATP binding (22) and pore gating (23). What is more important, it has allowed for a detailed characterization of the two structures and provided the first pictorial model for the closed-to-open transition. It has also been established that the system has a threefold symmetry around the transmembrane axis. Each chain crosses twice the lipid bilayer via two alpha-helix domains, TM1 and TM2. In addition, it has been assessed that the extracellular domain is large ($\approx$70 Å) when compared with the transmembrane domain ($\approx$25 Å). The shape of each subunit resembles that of a "dolphin." The bodies of the three dolphins cross each other above the membrane while the flukes overlap in the transmembrane region. The dolphins' "heads," "bodies," "flippers," and "dorsal fins" make up the extracellular domain. The "flukes" comprise the transmembrane domains.

Kinetic models for the opening of the channel have been proposed to explain the ionic currents generated in response to ultrafast ATP pulses (24–26). Based on these models, it has been suggested that an intermediate state exists in which the ATP is already bound while the channel is still closed. Further evidence of the existence of an intermediate state was provided later by Jiang et al. (27). The large amount of experimental research performed on these systems is in sharp contrast with the scarcity of computational studies presented so far. Normal mode analysis of the closed form has been conducted to identify collective motions that

Submitted April 14, 2016, and accepted for publication October 19, 2016.
*Correspondence: gsottile@unq.edu.ar
Editor: Carmen Domene
http://dx.doi.org/10.1016/j.bpj.2016.10.027

couple the binding of ATP with the opening of the pore (28,29). Docking and molecular dynamics (MD) simulations have also been used to analyze the alternative conformations that ATP and similar molecules can adopt when binding to the relatively large binding pocket (29,30).

In this article we present the results of extensive MD simulations of the closed structure of the $P2X_4$ receptor. The structural changes observed in these simulations are thoroughly examined and compared with those observed along the transition from the closed to the open structure. The main goal of the study is to shed light on the molecular details of the activation mechanism.

The rest of the article is organized as follows. We discuss the methods used to perform this work and provide details about the MD simulations in Materials and Methods. Here we describe the procedure we followed to split the motions of the receptor into intrachain deformations and interchain rigid-body movements. We also present details of the methodology used to determine the principal components of the closed form. In Results, we provide the outcomes of all the analyses and calculations. First we examine the differences between the minimized structures of the closed and open forms as well as the transition between them. Then, the dynamic aspects of the closed form are considered. We conclude with a discussion of these results and a summary of our main conclusions.

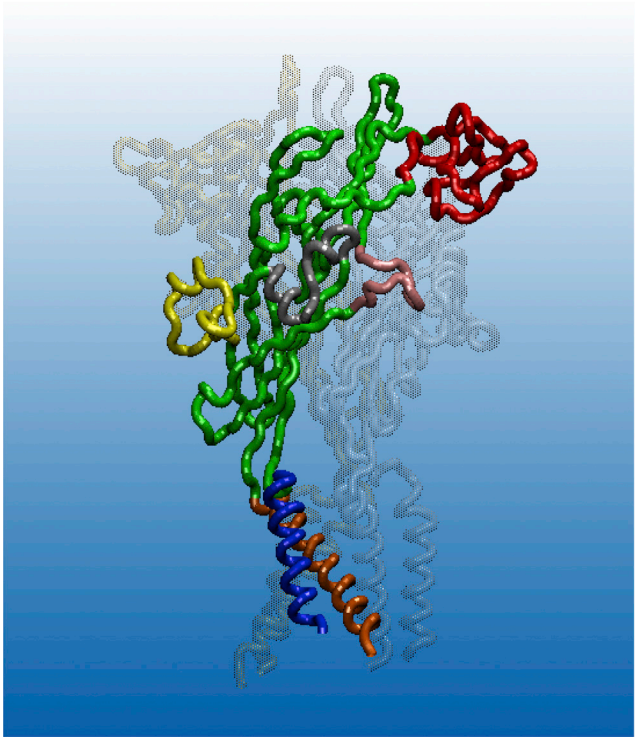

FIGURE 1 Single chain of the $P2X_4$ receptor. Kawate et al. (20) indicated that its form resembles that of a dolphin. The same pictorial description is employed in this work. Residues 31–55 belong to the TM1 region (*blue*); residues 56–112, 177–206, 231–234, 254–281, and 296–334 are the body (*green*); residues 113–176 are the head (*red*); residues 207–230 are the dorsal fin (*yellow*); residues 235–253 are the right flipper (*silver*); residues 282–295 are the left flipper (*magenta*); and residues 335–361 constitute the TM2 (*orange*). To see this figure in color, go online.

MATERIALS AND METHODS

Simulation details

The structures of the two conformations of the receptor were taken from the Protein Data Bank (PDB). They correspond to entries 3I5D (20) and 4DW1 (21), for the closed and open forms, respectively. Hereafter, the numbers of the residues and the names of the atoms are those found in these files. We present in Fig. 1 an illustration of a single chain. The different domains are colored and named according with the pictorial characterization proposed by Kawate et al. (20). The following paragraphs describe how the original PDB files were manipulated to produce chains of the same length so that they could be easily overlapped and compared.

The crystallographic structures lack ~30 residues at the N- and C-terminal parts. In the closed form, chain-A goes from Arg36 to Ile359, chain-B from Leu34 to Leu361, and chain-C from Leu34 to Trp358. Thus, we added residues 34, 35, 360, and 361 to chain-A, and residues 359–361 to chain-C, using chain-B as a template. The crystal structure of the open form, on the other hand, only contains one chain that goes from Arg36 to Ile359. We added to it residues 34, 35, 360, and 361 to obtain the same number of residues as the closed structure. The positions of the atoms for the other two chains were obtained by employing the symmetry information provided in the crystallographic data. In the structures so prepared, the length of the TM1 domains in the direction normal to the membrane plane is ~28Å. This is shorter than the usual thickness of a lipid bilayer (>30 Å). In addition, trial MD simulations of this protein model, embedded in a lipid bilayer, found that the structure is unstable. In particular, the N-terminal regions of each chain rotate, producing a noticeable change in the angle between the helices and the membrane normal. We assumed that this was caused by the missing residues at the N-terminal side. Therefore, we added residues Val31, Gly32, and Thr33 to all chains. The structure of the inserted segment was estimated using the I-TASSER server (31). It predicted that the new residues continue with the alpha helix motif of the residues already present. In the new protein models, the alpha helix of TM1 extends from residues 31 to 53, having a vertical length of ~32 Å that almost covers the thickness of the lipid bilayer.

We only performed MD simulations on the closed form of the channel. We utilized the graphical user interface of the CHARMM membrane builder (32,33) to soak the protein in a square lipid bilayer of 144.2 $Å^2$ that includes 512 POPC molecules (256 in each side). The protein was located so that the top of the membrane was aligned with residue Tyr52 of TM1. Water molecules were added to form an octahedral cell. The system was fed into the Leap module of Amber, selecting the Amber99SB force field to describe the protein plus the water molecules and the Lipid14 force field for the POPC molecules (34). The initial structure was minimized and then heated from 0 K to 100 K at constant volume during 120 ps. Next, the heating was continued from 100 K to 310 K during 120 ps, but switched to constant pressure conditions so that the density could relax. A harmonic restraint of 1.5 kcal/mol.$Å^2$ was applied on the C_α atoms of the protein and the oxygen atoms of the water molecules in the two heating periods. This was followed by four consecutive 100 ps simulations at 310 K in which the restraints were gradually eliminated (0.5, 0.1, 0.05, and 0.01 kcal/mol.$Å^2$). After that, we performed 25 consecutive MD simulations of 20 ps monitoring a correct density equilibration. With the model so prepared we performed eight equivalent MD simulations to assess the consistency of the results. All these simulations started from the same equilibrated structure and only differed in the initial atomic velocities, which were randomly chosen from a Maxwellian distribution at 310 K. The production phases of each simulation lasted for 200 ns, adding up a total of 1.6 μs. The SHAKE algorithm was implemented to constrain the length

of the bonds involving hydrogen atoms. This allowed for the use of a time step of 2.0 fs. A cutoff radius of 10.0 Å was employed for the nonbonded interactions. The particle mesh Ewald method was applied to handle the long-range coulombic forces (35,36).

Interchain and intrachain decomposition analysis

When describing the motions of a set of particles it is usually instructive to decompose them into two contributions. One of them is given by the translation and rotation of the whole set, considered as a rigid body. The second contribution comes from movements that modify the shape of the set of particles. These motions change the distances between particles and are usually referred to as the "internal" motions. The separation between rigid-body and internal motions is particularly enlightening when analyzing the fluctuations of oligomeric proteins. In this case, the rigid-body motions describe the interchain movements whereas the internal motions describe the intrachain movements (i.e., deformations of each chain). Recently, Vesper and de Groot presented a simple procedure to separate these two contributions (37). We implemented their method to study the fluctuations of the closed form of the $P2X_4$ receptor, as well as to analyze the *closed*→*open* transition. For completeness we briefly describe the procedure here.

With the snapshots collected from a MD simulation we proceed as follows. As usual, rigid-body translation and rotation of the whole protein are removed by least-square-fitting all the snapshots onto the first one. After that, for every snapshot, the C_α atoms of chain-A are least-square-fitted onto the C_α atoms of the same chain in the reference structure, and a new PDB file is recorded with the coordinates so generated. We used the minimized conformation of the closed form, $\mathbf{X}_{cl}^0$, as the reference structure. Altogether these PDB files describe a fictitious trajectory with the intrachain movements of chain-A. The procedure is repeated for the other two chains. When the PDB files of the three chains are merged, a trajectory with the intrachain movements of the whole protein is obtained. Hereafter, the set of structures of this fictitious trajectory will be denoted as $\{\mathbf{X}_{cl}^{intra}\}$, whereas $\mathbf{X}_{cl}^{intra}$ is a $3N$-dimensional vector containing the coordinates of the N atoms of the protein at a given snapshot. To obtain a fictitious trajectory with the interchain movements, we fit the C_α atoms of chain-A in the reference structure, $\mathbf{X}_{cl}^0$, onto the C_α atoms of chain-A in every snapshot, and we produce a new PDB file with the generated structures. The procedure is repeated for the other two chains and then the three PDB files are merged to produce the interchain trajectory of the whole protein. This fictitious trajectory is denoted as $\{\mathbf{X}_{cl}^{inter}\}$, whereas $\mathbf{X}_{cl}^{inter}$ refers to any of its snapshots.

It should be noted that the size of the conformational space of the interchain movements is significantly smaller than that of the intrachain movements. Six degrees of freedom are required to describe the rigid-body translations and rotations of each chain, thus requiring 18 degrees of freedom for the entire protein. However, because the translations and rotations of the whole system have been eliminated, six degrees of freedom are missed. Therefore, the interchain movements are described by just 12 degrees of freedom. The remaining $3N$-6-12 degrees of freedom span the intrachain conformational space, where N is the number of atoms considered.

The procedure used to decompose the snapshots of the MD trajectories into interchain and intrachain displacements was also applied to the *closed*→*open* transition. In this analysis we only employed the minimized structures of the closed and open forms, $\mathbf{X}_{cl}^0$ and $\mathbf{X}_{op}^0$. A PDB file with the coordinates obtained when only the intrachain *closed*→*open* transition occurs is generated by least-square-fitting each chain of $\mathbf{X}_{op}^0$ onto the corresponding chain in $\mathbf{X}_{cl}^0$. We denote the vector containing these coordinates as $\mathbf{X}_{op}^{intra}$. Similarly, a PDB file containing the coordinates generated when only the interchain *closed*→*open* transition occurs is obtained by least-square-fitting each chain of $\mathbf{X}_{cl}^0$ into the corresponding chain in $\mathbf{X}_{op}^0$. These coordinates are collected in the $\mathbf{X}_{op}^{inter}$ vector. Finally, by subtracting the coordinates contained in $\mathbf{X}_{cl}^0$ from those contained in $\mathbf{X}_{op}^{intra}$ and $\mathbf{X}_{op}^{inter}$, two $3N$ dimensional displacement vectors are obtained. One of them, $\mathbf{V}_{c\to o}^{intra} = \mathbf{X}_{op}^{intra} - \mathbf{X}_{cl}^0$, contains the coordinate changes that come along with the fictitious intrachain *closed*→*open* transition. The other one, $\mathbf{V}_{c\to o}^{inter} = \mathbf{X}_{op}^{inter} - \mathbf{X}_{cl}^0$, contains the coordinate changes in the fictitious intrachain *closed*→*open* transition.

Dynamical analysis and principal component analysis

We next thoroughly analyzed the dynamics of the closed form of the $P2X_4$ receptor. In particular we evaluated if the movements required to open the channel already occur, although to a lesser extent, in the closed structure. Also we performed a principal component analysis (PCA) of the fictitious trajectories $\{\mathbf{X}_{cl}^{intra}\}$ and $\{\mathbf{X}_{cl}^{inter}\}$. The correlation matrices used in this analysis only considered the Cartesian coordinates of the C_α atoms. The size of essential spaces, ES^{intra} and ES^{inter} was determined according to the following procedure. First, we calculated the atomic displacements from the average structure, for each configuration sampled in a MD simulation. Then we computed the inner products between the vectors containing such displacements and the successive Principal Component (PC) modes. A PC mode was considered to belong to the essential space if these inner products do not follow a Gaussian distribution (38). The normality of the distributions was evaluated by employing the Dangelo's test (39). Also, to assess the consistency between the data provided by the independent MD simulations, we computed the overlap between their covariance matrices (40,41). This parameter equals 1 if the subspaces sampled by two alternative simulations are the same and is 0 if they are orthogonal.

RESULTS

We next discuss the interactions and relative movements between two adjacent chains of the receptor, which we call A and B. Because of the symmetry of the system, the interactions between chains A and B are equivalent to those between B and C and between C and A. We always allude first to chain A and we refer to chain B as the "adjacent chain." In a view of the system from the extracellular side, perpendicular to the plane of the membrane, chain B is the first to be found when a counterclockwise rotation is performed starting from chain A.

Static aspects

Significant insights about the operation of the $P2X_4$ receptor have already been obtained from the comparison between the crystal structures of the closed and open forms (20,21). This analysis revealed that ATP promotes the closure of the binding site, producing the approach between the head of one chain and the dorsal fin of the adjacent chain. This movement, in turn, pushes the left flipper of the former chain out from the binding pocket. Because the left flipper and dorsal fin are tightly coupled to the lower body region, this causes a substantial expansion of the transmembrane channel.

With the aim of getting further insight into the nature of this coupling, we decomposed the *closed*→*open* transition vector into the fictitious transition vectors $\mathbf{V}_{c\to o}^{intra}$ and $\mathbf{V}_{c\to o}^{inter}$. In this process we first obtained the fictitious structures $\mathbf{X}_{op}^{intra}$ and $\mathbf{X}_{op}^{inter}$. Animations of the displacements observed in $\mathbf{V}_{c\to o}^{intra}$ and $\mathbf{V}_{c\to o}^{inter}$ are presented in Movies S1 and S2 in the Supporting Material, respectively. These

movies should be compared with those provided as supplementary information in (21), where the actual *closed*→*open* transition is shown. The $\mathbf{V}^{\text{intra}}_{c\to o}$ transition (Movie S1) shows that the distortion of the chains takes the head of chain A closer to the dorsal fin of chain B while, at the same time, it moves away from its upper body. In addition, the left flipper twists in a such way that its lower body gets closer to the middle body of chain B while its upper body drifts apart from the ATP binding site.

The animation of the $\mathbf{V}^{\text{inter}}_{c\to o}$ transition (Movie S2) indicates that the interchain movement also contributes to take the head of chain A closer to the dorsal fin of chain B. In addition, the left flipper of chain A gets closer to the bottom of the dorsal fin of chain B while it moves away from its middle and upper parts. Along with this movement, part of the head of chain A approaches the upper body of chain B.

In regard to the opening of the channel, the animations reveal that the interchain movement is mainly responsible for the widening of the transmembrane domain and low extracellular vestibule. To quantify this observation we estimated the expansion of the narrowest part of the transmembrane pore and the enlargement of the lower part of the extracellular vestibule, for each of the fictitious transitions. The size of the narrowest part of the transmembrane pore was measured by the distance between the central axis of the pore and the C_β atom of Ala347, excluding the Van der Waals radius. This distance changes from 0.8 to 3.60 Å along the complete *closed*→*open* transition. On the other hand, for the $\mathbf{V}^{\text{intra}}_{c\to o}$ transition it just reaches a value of 1.10 Å, whereas for $\mathbf{V}^{\text{inter}}_{c\to o}$ it reaches 3.26 Å. The extension of the lower extracellular domain was measured by the distance between the C_α atoms of the Asp59 residues belonging to contiguous chains. According to Hattori et al., this distance goes from 15.0 to 25.5 Å when the system switches from the closed to the open conformation (21). We found that this distance variates from 15.0 to 23.0 Å along $\mathbf{V}^{\text{inter}}_{c\to o}$ whereas it attains a value of just 17.9 Å along $\mathbf{V}^{\text{intra}}_{c\to o}$. Altogether, these results indicate that both, the interchain and the intrachain movements contribute to the conformational changes observed near the ATP binding site (head, left flipper, dorsal fin, and upper body regions). However, the widening of the fenestration region and the opening of the channel are mainly caused by the interchain movement contained in vector $\mathbf{V}^{\text{inter}}_{c\to o}$. Movie S2 shows that this movement can be fairly described as a rocking motion of the frozen chains.

We investigated the fictitious structures $\mathbf{X}^{\text{intra}}_{op}$ and $\mathbf{X}^{\text{inter}}_{op}$ to determine whether they contain clashes between atoms. The clashes that we spotted are presented in Tables 1 and 2 where we also indicate the location of these repulsive interactions. There are significantly less clashes along the $\mathbf{V}^{\text{intra}}_{c\to o}$ transition than along the $\mathbf{V}^{\text{inter}}_{c\to o}$ one. In the former case there are just six clashes. In the latter one there are 27, equally distributed between left flipper and middle body, upper body and upper body, and head and upper body. This is not surprising since these regions already contain many close contacts in the closed structure (20). It is nonetheless worthwhile to note that all clashes, both interchain and intrachain, occur away from the transmembrane domain. In other words, there are no steric impediments for the $\mathbf{V}^{\text{inter}}_{c\to o}$ or the $\mathbf{V}^{\text{intra}}_{c\to o}$ transitions at the lower body and transmembrane domains.

The main conclusions of this section are the following. The opening of the transmembrane pore is mainly caused by the interchain motions. To a good extent, they can be described as the rocking motions of the frozen chains. However, these movements cannot take place by themselves

TABLE 1 Van der Waals Clashes between Adjacent Chains Present in $\mathbf{X}^{\text{intra}}_{op}$

Chain A	Chain B
GLU98 (MB)	GLN97 (MB)
ARG143 (H)	THR218 (DF)
ARG280 (MB)	ASN204 (MB)
VAL291 (LF)	SER214 (DF)
ASP323 (MB)	SER66 (MB)
PHE327 (MB)	LEU64 (MB)

The domain to which each residue belongs is in parentheses: MB, middle body; H, head; DF, dorsal fin; LF, left flipper.

TABLE 2 Van der Waals Clashes between Adjacent Chains Present in $\mathbf{X}^{\text{inter}}_{op}$

Chain A	Chain B
GLN116 (H)	ARG85 (UB)
ASN140 (H)	LYS72 (UB)
ASP141 (H)	GLY73 (UB)
ALA142 (H)	LYS72 (UB)
ASP145 (H)	ASP88 (UB)
GLY146 (H)	ILE74 (UB)
LEU165 (H)	LEU76 (UB)
LEU165 (H)	ILE86 (UB)
SER166 (H)	ILE86 (UB)
TRP167 (H)	ARG85 (UB)
LEU282 (LF)	SER66 (MB)
ASN284 (LF)	ARG206 (MB)
ASN289 (LF)	ILE208 (DF)
ASN289 (LF)	LEU209 (DF)
ASN289 (LF)	PRO210 (DF)
ASN290 (LF)	ILE208 (DF)
VAL291 (LF)	LYS193 (MB)
ALA292 (LF)	LYS193 (MB)
PRO293 (LF)	LYS193 (MB)
TYR295 (LF)	ASP99 (MB)
ARG298 (UB)	ALA90 (UB)
ARG298 (UB)	GLN97 (UB)
ARG299 (UB)	GLN97 (UB)
PHE299 (UB)	ASP91 (UB)
ALA300 (UB)	ASP91 (UB)
TYR302 (UB)	LYS301 (UB)
ARG312 (UB)	ASP88 (UB)

The domain to which each residue belongs is in parentheses: MB, middle body; UP, upper body; H, head; LF, left flipper.

because they produce 27 severe Van der Waals clashes between each pair of chains. All these clashes are situated in the middle and upper part of the protein. The internal deformations of the chains, by themselves, also create Van der Waals clashes around the ATP binding site. When the two types of movements occur together, their detrimental effect cancels each other so that there are no clashes along the actual *closed*→*open* transition, as expected.

Dynamical aspects

The consistency of the results provided by the eight independent MD simulations was assessed by calculating the overlap between their covariance matrices. The equations employed for these calculations were proposed by Hess (40,41). For completeness, we provide them in the Supporting Material. We calculated the covariance overlap for the 28 pairs of matrices that can be formed from the 8 simulations. From this set, we computed an average overlap of 0.73 with a standard deviation of 0.08. This indicates that the individual simulations afford reasonably similar data.

The dynamical results reported here correspond to average values computed from the 8 independent 200-ns runs. When determining the PC modes and the projections of the trajectories onto ES^{inter} or ES^{intra}, each trajectory was analyzed individually. The data reported below are average values and standard deviations computed from these samples of eight data. For the rest of the MD results, we considered all the simulations together; that is, the snapshots collected from the eight simulations were used to form a single set from which averages and standard deviations were computed. Moreover, for interactions and distances that involve pairs of chains, the three possible pairs were considered. Therefore, the amount of data used to obtain such averages is three times the one used for averages corresponding to the whole protein.

Following the criteria explained above, we found that the size of the essential spaces ES^{inter} and ES^{intra} was three and six, respectively. It is normally assumed that the essential space of a protein contains the most relevant motions, those that are required to fulfill its function. Therefore we wondered to what extent ES^{intra} and ES^{inter} contain the directions required to perform the *closed*→*open* transition. To do so, we determined the square projection of $\tilde{\mathbf{v}}^{intra}_{c\to o}$ onto ES^{intra}, where $\tilde{\mathbf{v}}^{intra}_{c\to o}$ is a normalized vector in the direction of $\mathbf{V}^{intra}_{c\to o}$. Also, we computed the square projection of $\tilde{\mathbf{v}}^{inter}_{c\to o}$ onto ES^{inter}, where $\tilde{\mathbf{v}}^{inter}_{c\to o}$ is a normalized vector in the direction of $\mathbf{V}^{inter}_{c\to o}$. The $\tilde{\mathbf{v}}^{inter}_{c\to o}$ and $\tilde{\mathbf{v}}^{intra}_{c\to o}$ employed in these calculations only contained the coordinates of the C_α atoms so as to allow the projections on the PC modes. The equations used to evaluate the squared projections are presented in the Supporting Material. We found that the former projection is just 0.06 ± 0.05, whereas the second one is 0.72 ± 0.06. Both squared projections are larger than what would be obtained if all the degrees of freedom were equally likely (6/2961 = 0.003 for the intrachain subspace and 3/12 = 0.25 for the interchain subspace). Nevertheless, the most relevant information that emerges from this analysis is that the vectors spanning ES^{inter} are able to describe most of the displacements occurring along $\tilde{\mathbf{v}}^{inter}_{c\to o}$. Vector $\tilde{\mathbf{v}}^{intra}_{c\to o}$, on the other hand, is almost perpendicular to ES^{intra}.

Visually, the similarity between the displacements observed in $\mathbf{V}^{inter}_{c\to o}$ and the interchain fluctuations observed in the MD simulations can be appreciated by comparing Movie S2, which contains the animation of $\mathbf{V}^{inter}_{c\to o}$, with Movie S3, which contains the animation of the first eigenvector of the interchain modes.

We want to highlight the importance of performing the interchain/intrachain separation. Without this analysis tool, the fact that the opening of the channel is mainly attributable to the interchain movement would have been masked. The procedure also allowed us to reveal that ES^{inter} mostly contains the direction of the interchain *closed*→*open* transition. If a PCA is performed without applying the decomposition, the squared projection of $\tilde{\mathbf{v}}_{c\to o}$ onto the subspace formed by the first six PC modes is just 0.11 ± 0.05. If the first nine modes are considered, the squared projection increases to 0.14 ± 0.06.

The previous analysis shows that almost none of $\mathbf{V}^{intra}_{c\to o}$ is contained in ES^{intra} whereas an important part of $\mathbf{V}^{inter}_{c\to o}$ lies in ES^{inter}. However, this does not tell us to what extent the required fluctuations actually occur. To investigate this issue we subtracted the minimized structure of the closed form, $\mathbf{X}^0_{cl}$, from the fictitious interchain trajectory contained in $\{\mathbf{X}^{inter}_{cl}\}$. Then, we calculated the inner product between the instantaneous displacements and $\tilde{\mathbf{v}}^{inter}_{c\to o}$. This gives the actual displacements of the interchain movements along the direction of $\mathbf{V}^{inter}_{c\to o}$. By dividing these numbers by the magnitude of vector $\mathbf{V}^{inter}_{c\to o}$ we calculated what fraction of the required displacement is really achieved. The time evolution of these inner products, for two typical trajectories, is presented in Fig. 2. Similar plots are obtained when the other simulations are considered. It is seen that, in the most favorable situations, the actual fluctuations only cover ~25% of the whole interchain *closed*→*open* transition. In other words, even though ES^{inter} contains a significant fraction of $\mathbf{V}^{inter}_{c\to o}$, the interchain fluctuations observed in typical MD simulations of the closed form are restrained and only cover a tiny amount of the displacements required for the opening.

These results corroborate that a naive vision, which assumes that the real transition smoothly interpolates between the closed and open conformations, is incorrect. Instead, a defined sequence of conformational changes, occurring at different parts of the protein, is required. Recently, an elegant and detailed computational study was able to reveal such a sequence of conformational changes for a membrane transporter (42). In this context, we wondered what interactions restrained the interchain movements in the absence of the intrachain deformations. Clearly, those intrachain

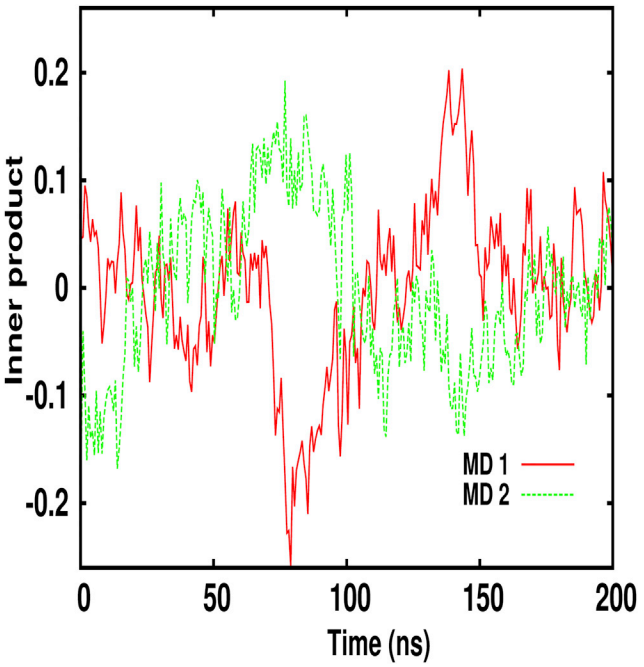

FIGURE 2 Inner product between vector $(\mathbf{X}_{cl}^{inter}(t) - \mathbf{X}_{cl}^{0})/\left|\mathbf{V}_{c\to o}^{inter}\right|$ and versor $\tilde{\mathbf{v}}_{c\to o}^{inter}$ for the snapshots collected along two MD simulations. Similar plots are obtained with the other simulations. To see this figure in color, go online.

conformational changes must occur in the first place to unlock the interchain movement. The restraints can come from the loss of attractive interactions and/or from the formation of repulsive interactions. We examined these two possibilities below.

To explore the repulsive interactions, we first selected pairs of atoms that, belonging to adjacent chains, were in close contact along the MD simulation (average distance <3.5Å). Then, from this set, we identified those pairs whose distance in $\mathbf{X}_{op}^{inter}$ were smaller than their smallest distance in $\{\mathbf{X}_{cl}^{inter}\}$. The reasoning behind this selection criterion is that fluctuations in $\{\mathbf{X}_{cl}^{inter}\}$ and $\{\mathbf{X}_{cl}^{intra}\}$ compensate to each other so that, in the MD simulations, the pairs of atoms are in close contact but do not overlap. Accordingly, any shorter distance observed in $\mathbf{X}_{op}^{inter}$ would not be compensated by the intrachain deformations naturally occurring in the absence of ATP. These interactions would, at some point, hinder and eventually stop the interchain movements required to open the channel. The pairs of atoms that fulfill these criteria are presented in Table 3.

The consistency of the interacting pairs identified with the criteria described above was assessed by employing the following alternative procedure. We generated fictitious structures by linearly interpolating between $\mathbf{X}_{cl}^{0}$ and $\mathbf{X}_{op}^{inter}$. Then we spotted the clashes that take place along such transformations. The pairs of atoms shown in Table 3 are the first to show up when one follows this procedure. They all appear just before 20% of the whole transition has occurred.

Table 3 shows that the selected interatomic distances are rather similar in the actual closed and open structures. However, the comparison of the average separations in the fictitious trajectories of the closed form, $\{\mathbf{X}_{cl}^{inter}\}$ and $\{\mathbf{X}_{cl}^{intra}\}$, with the separations in the fictitious open structures, $\mathbf{X}_{op}^{inter}$ and $\mathbf{X}_{op}^{intra}$, reveals that this agreement is achieved in different ways. The distances sampled from $\{\mathbf{X}_{cl}^{inter}\}$ are large. However, because they get small values in $\{\mathbf{X}_{cl}^{intra}\}$, the pairs are just kept in close contact. According to the data of the seventh column of the table, the interchain *closed*→*open* transition leaves the same pairs of atoms too close to each other, but this is compensated by the distortions that occur along the intrachain *closed*→*open* transition, which separates them considerably. The results of the MD simulations demonstrate that these distortions do not occur in the absence of ATP. Therefore, the interchain movement is impeded.

To investigate the attractive interactions, we analyzed the behavior of the most significant H-bonds between adjacent chains. We considered as "significant" those H-bonds that were present in more than 50% of the conformations sampled in the MD trajectory. Table 4 displays the interactions that fulfill with this criterion. None of them are present in either $\mathbf{X}_{op}^{inter}$ or $\mathbf{X}_{op}^{intra}$, but a couple of them are still present in the actual open structure. These are Gln116-Ile86 and Arg312-Asp88. On the other hand, Glu310-Arg85, present in the closed structure, is replaced by Glu310-Lys301 and Glu310-Tyr303 in the real open structure. The rest of the attractive interactions are disrupted. In particular, all the H-bonds between the left flipper of one chain and the dorsal fin of the adjacent chain are broken. In the open structure, these domains interact with the ATP molecule.

TABLE 3 Distances between Pair of Atoms that Experience the Largest Repulsive Interactions along the Fictitious Interchain *closed*→*open* Transition

Chain A	Chain B	$\langle d_{cl}\rangle$ (Å)	$\langle d_{cl}^{inter}\rangle$ (Å)	$\langle d_{cl}^{intra}\rangle$ (Å)	d_{op} (Å)	d_{op}^{inter} (Å)	d_{op}^{intra} (Å)
GLN116NE2 (H)	ARG85NH (UB)	3.48 ± 0.63	4.23 ± 0.46	3.24 ± 0.71	4.16	1.65	5.70
ASN289ND2 (LF)	LEU209O (DF)	3.26 ± 0.64	3.51 ± 0.24	3.42 ± 0.40	4.56	3.01	7.82
ALA292O (LF)	LYS193NZ (MB)	3.29 ± 0.58	3.52 ± 0.38	3.19 ± 0.40	3.00	0.58	5.89

The data corresponding to the closed form were computed by averaging together the results of the eight independent MD simulations. The errors indicate the standard deviations. The domain to which each residue belongs is in parentheses: MB refers to middle body; UP to the upper body; H to head; DF to dorsal fin; and LF to left flipper.

TABLE 4 Average Occupancy of the Interchain H-bonds that Are Present in More than 50% of the Conformations Sampled along the Eight MD Simulations Considered Altogether

Chain A	Chain B	% MD traj
GLN116 (H)	ILE86 (UB)	61.4 ± 1.0
ASP141 (H)	ILE74 (UB)	51.1 ± 0.7
PRO287 (LF)	SER214 (DF)	57.8 ± 1.2
ASN289 (LF)	LEU209 (DF)	71.7 ± 1.1
ASN290 (LF)	SER214 (DF)	51.2 ± 1.2
GLU310 (UB)	ARG85 (UB)	76.7 ± 0.8
ARG312 (UB)	ASP88 (UB)	81.9 ± 1.4
ASP323 (UB)	SER66 (UB)	59.8 ± 0.7

The errors indicate the standard deviations. The domain to which each residue belongs is in parentheses: UB, upper body; H, head; DF, dorsal fin; LF, left flipper.

A clear pattern is evident when the repulsive and attractive interactions are examined collectively. Thus one realizes that, with the exception of the interaction between Asp323 and Ser66, all the other pairs are in two specific regions of the system, located immediately above and below the ATP binding zone. These two regions are represented in Fig. 3. One of them corresponds to the contact between the left flipper of chain A and the dorsal fin of chain B. The other one corresponds to the contact between the upper body and head of chain A with the upper body of chain B. The importance of the interactions between these regions has already been revealed in numerous experimental studies (28,30,43–45). In particular, Tvrdonova et al. (43) have indicated that residues in the left flipper and dorsal fin domains could be involved, not only in ATP recognition and binding, but also in signal transduction.

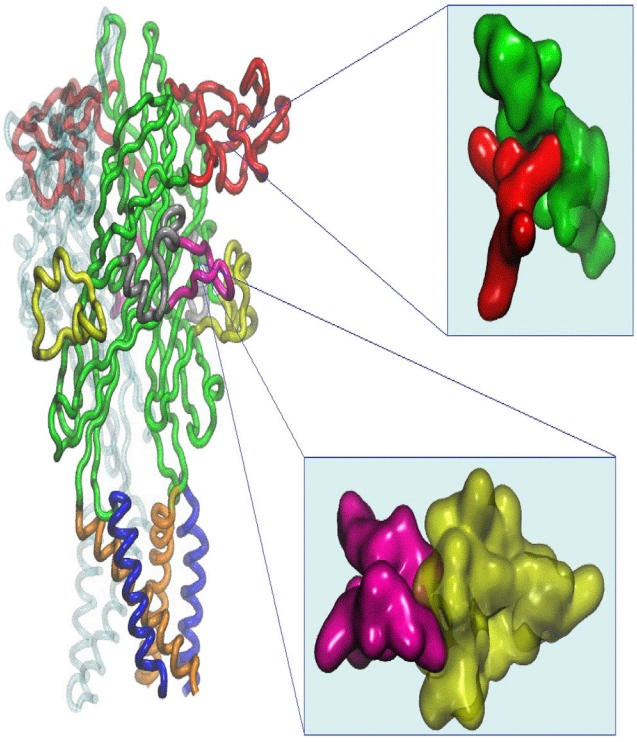

FIGURE 3 Zones of the system most affected by the fictitious $\mathbf{V}^{\text{inter}}_{c\to o}$ transition. Significant interchain H-bonds are broken and severe interchain van der Waals clashes are formed in these regions if only the $\mathbf{V}^{\text{inter}}_{c\to o}$ transition occurs. To see this figure in color, go online.

From the previous analysis, it can be inferred that the distances between adjacent chains, at the key locations described above, should change in an anticorrelated way in the fictitious trajectories $\{\mathbf{X}^{\text{inter}}_{\text{cl}}\}$ and $\{\mathbf{X}^{\text{intra}}_{\text{cl}}\}$ so that an appropriate distance between the interacting pairs can be maintained. To verify this, we evaluated the separation between the dorsal fin of chain A (residues Pro287-Ala292) and the left flipper of chain B (residues Pro210-Ser214). The residues belonging to these parts have already been specified in the caption of Fig. 1. Similarly, we evaluated the separation between the upper body of one chain (residues Glu84-Asp88) and head plus the upper body of the adjacent chain (residues Glu310-Arg312 and Gln114-Lys118). The separations between groups were estimated by the distances between the centers of mass of their C_α atoms. In Fig. 4 the results are shown. The plots clearly indicate that the movement in these two regions of the system is, as expected, strongly anticorrelated.

DISCUSSION

The dynamics of any oligomeric protein can be decomposed as an interchain motion that describes the translation and rotation of the chains, considered as rigid bodies, plus an intrachain motion that describes their internal deformations. We applied such decomposition to the *closed*→*open* transition of the $P2X_4$ receptor and found that the opening of the

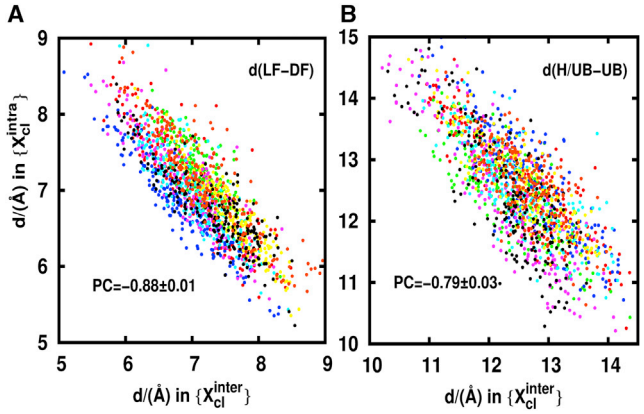

FIGURE 4 Correlation plot for selected distances along the interchain and intrachain movements. (*A*) Distances between the left flipper (LF) and dorsal fin (DF) of contiguous chains are shown. (*B*) Distances between the head/upper body (H/UB) and the upper body (UB) of contiguous chains are shown. Different colors were assigned to each MD simulation. The Pearson's coefficient (PC) was computed for each MD simulation and the provided value corresponds to the average coefficient. The errors measure the standard deviation. For the sake of clarity only one-tenth of the data were plotted. To see this figure in color, go online.

transmembrane pore is mostly caused by the interchain displacements. A visual inspection of these movements shows that they can be fairly described as rocking motions. When the head of the chain moves down, the TM helices move outward, opening the channel. Contrarily, when the head moves up the TM helices move inward closing the channel.

On the other hand, the interchain movements observed in the eight independent MD simulations of the closed form were found to have similar directions than those seen in the *closed*→*open* transition. However, in the absence of ATP, these movements cannot achieve the amplitude required to open the pore because they produce severe van der Waals clashes and destroy important H-bond interactions between adjacent chains. These van der Waals clashes and H-bonds are in two critical regions located around the ATP binding site. One region involves the interaction between the left flipper of chain A and the dorsal fin of chain B. The other one involves the interaction between head and upper body of chain A with the upper body of chain B.

Several MD studies performed on other proteins have reported that the movements required for the transition from the inactive to the active conformation are already present in the inactive form. This includes both, membrane and nonmembrane proteins (46–54). However, as far as we know, this is the first case in which the analysis is performed after decomposing the atomic displacements into interchain and intrachain movements. This decomposition turned out to be crucial since only the interchain movements are "encoded" into the closed form of the $P2X_4$ receptor. Without the decomposition this fact would have been masked.

A closer look into the dynamics of the closed form demonstrated that the interchain and intrachain movements changed the distances between important domains in an anticorrelated way. Therefore, their effects compensate to each other so that the actual distances are maintained within an appropriate range. This suggests that the even larger interchain displacements required to open the pore cannot occur because the intrachain deformations observed in the absence of ATP are not able to compensate them. According to this view, one of the actions of the ATP would be to reshape the interactions that hinder the interchain motions, so that the rocking of the chains can achieve the amplitude needed to open the pore.

CONCLUSIONS

We have presented a detailed MD study of the closed form of the $P2X_4$ receptor. The comparison between the displacements observed in the MD simulation and those occurring along the *closed*→*open* transition provided some indications about the gating mechanism and the role played by the ATP. It was established that the opening of the pore is mainly caused by a rocking motion of the chains, considered as rigid bodies. This motion partly occurs when $P2X_4$ is closed. However, under such conditions, the rocking motion does not achieve enough amplitude because is impeded by interactions between adjacent chains. All these interactions take place around the ATP binding site. This suggests that one of the effects of the binding of ATP would be to release the restrains that hinder the rocking motion. Further computational or experimental studies are needed to confirm or rebut this hypothesis.

SUPPORTING MATERIAL

Supporting Materials and Methods and three movies are available at http://www.biophysj.org/biophysj/supplemental/S0006-3495(16)30956-0.

AUTHOR CONTRIBUTIONS

G.P.S. and J.P. conceived and designed the calculations. G.P.S. performed the experiments. G.P.S., L.M., and J.P. analyzed the data. G.P.S., L.M., and J.P. contributed equipment/analysis tools. G.P.S. and J.P. wrote the article.

ACKNOWLEDGMENTS

The authors want to thank CONICET for the financial support and Prof. Dr. Santiago de Rosa for enlightening discussions on this project. Financial and computational support from the Universidad Nacional de Quilmes is also gratefully acknowledged.

REFERENCES

1. Khakh, B. S., and R. A. North. 2006. P2X receptors as cell-surface ATP sensors in health and disease. *Nature.* 442:527–532.
2. Surprenant, A., and R. A. North. 2009. Signaling at purinergic P2X receptors. *Annu. Rev. Physiol.* 71:333–359.
3. Edwards, F. A., A. J. Gibb, and D. Colquhoun. 1992. ATP receptor-mediated synaptic currents in the central nervous system. *Nature.* 359:144–147.
4. Khakh, B. S., and G. Henderson. 1998. ATP receptor-mediated enhancement of fast excitatory neurotransmitter release in the brain. *Mol. Pharmacol.* 54:372–378.
5. Finger, T. E., V. Danilova, …, S. C. Kinnamon. 2005. ATP signaling is crucial for communication from taste buds to gustatory nerves. *Science.* 310:1495–1499.
6. Cook, S. P., L. Vulchanova, …, E. W. McCleskey. 1997. Distinct ATP receptors on pain-sensing and stretch-sensing neurons. *Nature.* 387:505–508.
7. Cockayne, D. A., S. G. Hamilton, …, A. P. D. W. Ford. 2000. Urinary bladder hyporeflexia and reduced pain-related behaviour in $P2X_3$-deficient mice. *Nature.* 407:1011–1015.
8. Galligan, J. J. 2004. Enteric P2X receptors as potential targets for drug treatment of the irritable bowel syndrome. *Br. J. Pharmacol.* 141:1294–1302.
9. Miller, C. M., N. R. Boulter, …, N. C. Smith. 2011. The role of the $P2X_7$ receptor in infectious Diseases. *PLoS Pathog.* 7:e1002212.
10. Chessell, I. P., J. P. Hatcher, …, G. N. Buell. 2005. Disruption of the $P2X_7$ purinoceptor gene abolishes chronic inflammatory and neuropathic pain. *Pain.* 114:386–396.
11. Fabre, J.-E., M. Nguyen, …, B. H. Koller. 1999. Decreased platelet aggregation, increased bleeding time and resistance to thromboembolism in $P2Y_1$-deficient mice. *Nat. Med.* 5:1199–1202.

12. Jelassi, B., A. Chantôme, …, S. Roger. 2011. $P2X_7$ receptor activation enhances SK3 channels- and cystein cathepsin-dependent cancer cells invasiveness. *Oncogene.* 30:2108–2122.
13. Adinolfi, E., M. Capece, …, A. Franceschini. 2015. Emerging roles of P2X receptors in cancer. *Curr. Med. Chem.* 22:878–890.
14. Browne, L. E., L. H. Jiang, and R. A. North. 2010. New structure enlivens interest in P2X receptors. *Trends Pharmacol. Sci.* 31:229–237.
15. Romagnoli, R., P. G. Baraldi, …, S. Gessi. 2008. The $P2X_7$ receptor as a therapeutic target. *Expert Opin. Ther. Targets.* 12:647–661.
16. Burnstock, G., and C. Kennedy. 2011. P2X receptors in health and disease. *Adv. Pharmacol.* 61:333–372.
17. Bean, B. P. 1990. ATP-activated channels in rat and bullfrog sensory neurons: concentration dependence and kinetics. *J. Neurosci.* 10:1–10.
18. Nicke, A., H. G. Bäumert, …, G. Schmalzing. 1998. $P2X_1$ and $P2X_3$ receptors form stable trimers: a novel structural motif of ligand-gated ion channels. *EMBO J.* 17:3016–3028.
19. North, R. A. 2002. Molecular physiology of P2X receptors. *Physiol. Rev.* 82:1013–1067.
20. Kawate, T., J. C. Michel, …, E. Gouaux. 2009. Crystal structure of the ATP-gated $P2X_4$ ion channel in the closed state. *Nature.* 460:592–598.
21. Hattori, M., and E. Gouaux. 2012. Molecular mechanism of ATP binding and ion channel activation in P2X receptors. *Nature.* 485:207–212.
22. Jiang, L.-H., F. Rassendren, …, R. A. North. 2000. Identification of amino acid residues contributing to the ATP-binding site of a purinergic P2X receptor. *J. Biol. Chem.* 275:34190–34196.
23. Jiang, R., A. Martz, …, T. Grutter. 2010. A putative extracellular salt bridge at the subunit interface contributes to the ion channel function of the ATP-gated P2X2 receptor. *J. Biol. Chem.* 285:15805–15815.
24. Ding, S., and F. Sachs. 1999. Single channel properties of $P2X_2$ purinoceptors. *J. Gen. Physiol.* 113:695–720.
25. Moffatt, L. 2007. Estimation of ion channel kinetics from fluctuations of macroscopic currents. *Biophys. J.* 93:74–91.
26. Moffatt, L., and R. I. Hume. 2007. Responses of rat $P2X_2$ receptors to ultrashort pulses of ATP provide insights into ATP binding and channel gating. *J. Gen. Physiol.* 130:183–201.
27. Jiang, R., A. Taly, …, T. Grutter. 2012. Intermediate closed channel state(s) precede(s) activation in the ATP-gated P2X2 receptor. *Channels (Austin).* 6:398–402.
28. Jiang, R., A. Taly, …, T. Grutter. 2012. Tightening of the ATP-binding sites induces the opening of P2X receptor channels. *EMBO J.* 31:2134–2143.
29. Du, J., H. Dong, and H.-X. Zhou. 2012. Gating mechanism of a $P2X_4$ receptor developed from normal mode analysis and molecular dynamics simulations. *Proc. Natl. Acad. Sci. USA.* 109:4140–4145.
30. Huang, L.-D., Y.-Z. Fan, …, Y. Yu. 2014. Inherent dynamics of head domain correlates with ATP-recognition of P2X4 receptors: insights gained from molecular simulations. *PLoS One.* 9:e97528.
31. Roy, A., A. Kucukural, and Y. Zhang. 2010. I-TASSER: a unified platform for automated protein structure and function prediction. *Nat. Protoc.* 5:725–738.
32. Jo, S., J. B. Lim, …, W. Im. 2009. CHARMM-GUI Membrane Builder for mixed bilayers and its application to yeast membranes. *Biophys. J.* 97:50–58.
33. Wu, E. L., X. Cheng, …, W. Im. 2014. CHARMM-GUI Membrane Builder toward realistic biological membrane simulations. *J. Comput. Chem.* 35:1997–2004.
34. Dickson, C. J., B. D. Madej, …, R. C. Walker. 2014. Lipid14: the Amber lipid force field. *J. Chem. Theory Comput.* 10:865–879.
35. Darden, T., D. York, and L. Pedersen. 1993. Particle mesh Ewald: an N log(N) method for Ewald sums in large systems. *J. Chem. Phys.* 98:10089–10092.
36. Essmann, U., L. Perera, …, L. G. Pedersen. 1995. A smooth particle mesh Ewald method. *J. Chem. Phys.* 103:8577–8593.
37. Vesper, M. D., and B. L. de Groot. 2013. Collective dynamics underlying allosteric transitions in hemoglobin. *PLOS Comput. Biol.* 9:e1003232.
38. Amadei, A., A. B. M. Linssen, and H. J. C. Berendsen. 1993. Essential dynamics of proteins. *Proteins.* 17:412–425.
39. D'Agostino, R. B., A. Belanger, and R. B. D'Agostino, Jr. 1990. A suggestion for using powerful and informative tests of normality. *Am. Stat.* 44:316–321.
40. Hess, B. 2000. Similarities between principal components of protein dynamics and random diffusion. *Phys. Rev. E.* 62:8438–8448.
41. Hess, B. 2002. Convergence of sampling in protein simulations. *Phys. Rev. E Stat. Nonlin. Soft Matter Phys.* 65:031910.
42. Moradi, M., and E. Tajkhorshid. 2013. Mechanistic picture for conformational transition of a membrane transporter at atomic resolution. *Proc. Natl. Acad. Sci. USA.* 110:18916–18921.
43. Tvrdonova, V., M. B. Rokic, …, H. Zemkova. 2014. Identification of functionally important residues of the rat P2X4 receptor by alanine scanning mutagenesis of the dorsal fin and left flipper domains. *PLoS One.* 9:e112902.
44. Lörinczi, É., Y. Bhargava, …, A. Nicke. 2012. Involvement of the cysteine-rich head domain in activation and desensitization of the P2X1 receptor. *Proc. Natl. Acad. Sci. USA.* 109:11396–11401.
45. Yan, Z., Z. Liang, …, S. S. Stojilkovic. 2005. Molecular determinants of the agonist binding domain of a P2X receptor channel. *Mol. Pharmacol.* 67:1078–1088.
46. Shrivastava, I. H., and I. Bahar. 2006. Common mechanism of pore opening shared by five different potassium channels. *Biophys. J.* 90:3929–3940.
47. de Groot, B. L., G. Vriend, and H. J. Berendsen. 1999. Conformational changes in the chaperonin GroEL: new insights into the allosteric mechanism. *J. Mol. Biol.* 286:1241–1249.
48. Berendsen, H. J., and S. Hayward. 2000. Collective protein dynamics in relation to function. *Curr. Opin. Struct. Biol.* 10:165–169.
49. Bakan, A., and I. Bahar. 2009. The intrinsic dynamics of enzymes plays a dominant role in determining the structural changes induced upon inhibitor binding. *Proc. Natl. Acad. Sci. USA.* 106:14349–14354.
50. de Groot, B. L., X. Daura, …, H. Grubmüller. 2001. Essential dynamics of reversible peptide folding: memory-free conformational dynamics governed by internal hydrogen bonds. *J. Mol. Biol.* 309:299–313.
51. Lange, O. F., N.-A. Lakomek, …, B. L. de Groot. 2008. Recognition dynamics up to microseconds revealed from an RDC-derived ubiquitin ensemble in solution. *Science.* 320:1471–1475.
52. Bahar, I., T. R. Lezon, …, I. H. Shrivastava. 2010. Normal mode analysis of biomolecular structures: functional mechanisms of membrane proteins. *Chem. Rev.* 110:1463–1497.
53. Temiz, N. A., and I. Bahar. 2002. Inhibitor binding alters the directions of domain motions in HIV-1 reverse transcriptase. *Proteins.* 49:61–70.
54. Horstink, L. M., R. Abseher, …, C. W. Hilbers. 1999. Functionally important correlated motions in the single-stranded DNA-binding protein encoded by filamentous phage Pf3. *J. Mol. Biol.* 287:569–577.